Label-free monitoring of proteins in optofluidic hollow-core photonic crystal fibres

Jan R. Heck,[ab] Ermanno Miele,[ab] Ralf Mouthaan,[ac] Michael H. Frosz,[d] Tuomas P.J. Knowles,[ab] Tijmen G. Euser*[a]
[a] Department of Physics, Cavendish Laboratory, University of Cambridge, UK
[b] Yusuf Hamied Department of Chemistry, University of Cambridge, UK
[c] Department of Electrical Engineering, University of Cambridge, UK
[d] Max Planck Institute for the Science of Light, Erlangen, DE

(Author list omitted for peer review)

Received xxxxxx
Accepted for publication xxxxxx
Published xxxxxx

Abstract

The fluorescent detection of proteins without labels or stains, which affect their behaviour and require additional genetic or chemical preparation, has broad applications to biological research. However, standard approaches require large sample volumes or analyse only a small fraction of the sample. Here we use optofluidic hollow-core photonic crystal fibres to detect and quantify sub-microlitre volumes of unmodified bovine serum albumin (BSA) protein down to 100 nM concentrations. The optofluidic fibre's waveguiding properties are optimised for guidance at the (auto)fluorescence emission wavelength, enabling fluorescence collection from a 10 cm long excitation region, increasing sensitivity. The observed spectra agree with spectra taken from a conventional cuvette-based fluorimeter, corrected for the guidance properties of the fibre. The BSA fluorescence depended linearly on BSA concentration, while only a small hysteresis effect was observed, suggesting limited biofouling of the fibre sensor. Finally, we briefly discuss how this method could be used to study aggregation kinetics. With small sample volumes, the ability to use unlabelled proteins, and continuous flow, the method will be of interest to a broad range of protein-related research.

Keywords: hollow-core photonic crystal fibre (HC-PCF), fibre, intrinsic fluorescence, autofluorescence, label-free, protein, intrinsic protein fluorescence, biophysics, optofluidics, waveguide, 280nm, tryptophan, microfluidics, antiresonant hollow-core fibre (AR-HCF), single-ring fibre, microstructured optical fibre (MOF)

Introduction

Proteins are the universal building blocks of biology, and understanding changes in their state is central to understanding life. Diseases associated with minor changes in protein structure are, among many others, protein folding disorders such as Alzheimer's or Parkinson's.[1]

Proteins change over time, either reversibly (conformation) or irreversibly (aggregation), and continuous monitoring of their properties is essential to understanding their behaviour. Furthermore, to study how proteins react to changes in their environment – for example, the presence of (drug) molecules – measurements should ideally be conducted under flow to allow for uninterrupted observation while changes occur. Real-time monitoring is particularly relevant for processes happening on short timescales, e.g. the initial monomer aggregation of amyloid-β typically occurs in under 5 minutes.[2] Additionally, discrete sampling and offline measurements can perturb the sample, and their sensitivity to

the chemical environment means that proteins are preferably studied in their unmodified, native state without fluorescent stains or labels.[3]

1.1 Intrinsic fluorescence for protein analysis

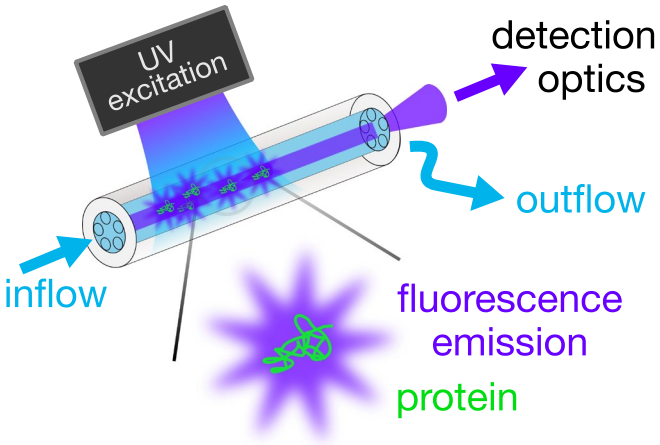

Figure 1 Concept of using optofluidic waveguides for label-free fluorescence collection. A sample solution containing unlabelled proteins flows through a HC-PCF. The aromatic residue tryptophan in the proteins is excited transversely using UV (275 nm) LEDs. The emitted fluorescence ($\lambda \approx$ 350 nm) is collected over the entire excitation region, guided by waveguide modes to the distal end of the HC-PCF, and directed to detection optics (see Fig. 2).

Fluorescent labels are commonly used for the optical detection of proteins.[4–6] Fluorophores can be incorporated into proteins by genetic modification, covalent attachment, or van-der-Waals interactions. Fluorescent labels allow for high specificity and sensitivity[7] and have previously enabled the first single-biomolecule studies.[8] Despite these excellent sensing properties, labels have been identified to significantly interfere with the proteins' behaviour, including their dimerisation[9] and aggregation[10]. This has driven the development of new label-free detection methods.

Most proteins exhibit intrinsic (label-free) fluorescence when excited in the UV wavelength range. The active groups are typically aromatic residues in their peptide chain. For example, tryptophan accounts for ca. 1 % [11] of the amino acids in proteins, such that proteins larger than one hundred amino acids are likely to contain at least one intrinsic fluorophore. Intrinsic fluorescence can act as an indicator of protein conformation, since conformation changes the exposure of tryptophan to the solvent, quenching fluorescence emission to different degrees.[12,13] This allows information on the current folding state of tryptophan within the protein to be extracted from their fluorescence intensity, wavelength, polarisation and lifetime. [14–16]

1.2 Studying proteins label-free

Continuous-flow microfluidic systems are ideal for studies of protein aggregation and conformation in the presence of small-molecule drugs, as they enable real-time analysis of small-volume samples. Optical detection in such systems is typically performed with a fluorescence microscope that transversely probes a thin fluidic channel. While this approach works well for labelled proteins, there are major challenges to performing intrinsic fluorescence measurements in such systems. First, intrinsic fluorescence is much weaker than that of labels, resulting in very low count rates when probing a thin layer of sample. Second, the excitation wavelength for intrinsic fluorescence is typically in the 250-300 nm range, resulting in strong background fluorescence from typical microfluidic chip materials such as PDMS. As a result, label-free fluorescence detection in standard microfluidic chips has focused on aggregated structures at higher concentrations, for example, in microdroplet arrays containing 6.9 mM lysozyme that form fibrils after 10 h of aggregation.[17] Recent improvements to these methods include extensive image post-processing and the addition of carbon black to the PDMS to reduce background fluorescence, but measurements still required a relatively high protein concentration (0.5 µM BSA) due to the inherently short detection path.[18]

1.3 Optofluidic waveguides for fluorescence detection

An excellent approach to increasing the detection path length is integrating the flow channel with an optical waveguide. Such optofluidic waveguides have been realised in a range of different materials and geometries[19]. In our experiments, it is essential to use weakly fluorescent materials such as fused silica to reduce background fluorescence. Glass microcapillaries can act as hollow waveguides. However, their guidance is typically very lossy due to the absence of total internal reflection. As a result, their attenuation scales as $\lambda^2 r^{-3}$, and path lengths typically do not exceed a few mm for a bore radius of 5 µm.[20] Another approach that has been tried to combine glass waveguides into microfluidics is embedding solid-core fibres within a microfluidic channel.[21] The sensitivity of such a system is limited as the excitation is evanescent (short-range), and the fluorescence is not collected over the entire excitation region. Similarly, the reverse approach of embedding a microfluidic channel into a solid-core fibre has been studied for biosensing, detecting concentrations of BSA protein above 0.2 mg/mL (3 µM).[22]

Hollow-core photonic crystal fibres (HC-PCF) are special optical fibres that overcome the high waveguide losses by surrounding a central hollow channel with a glass microstructure. The microstructure uses interference effects to reflect light, resulting in a hollow waveguide with minimal losses.[23]

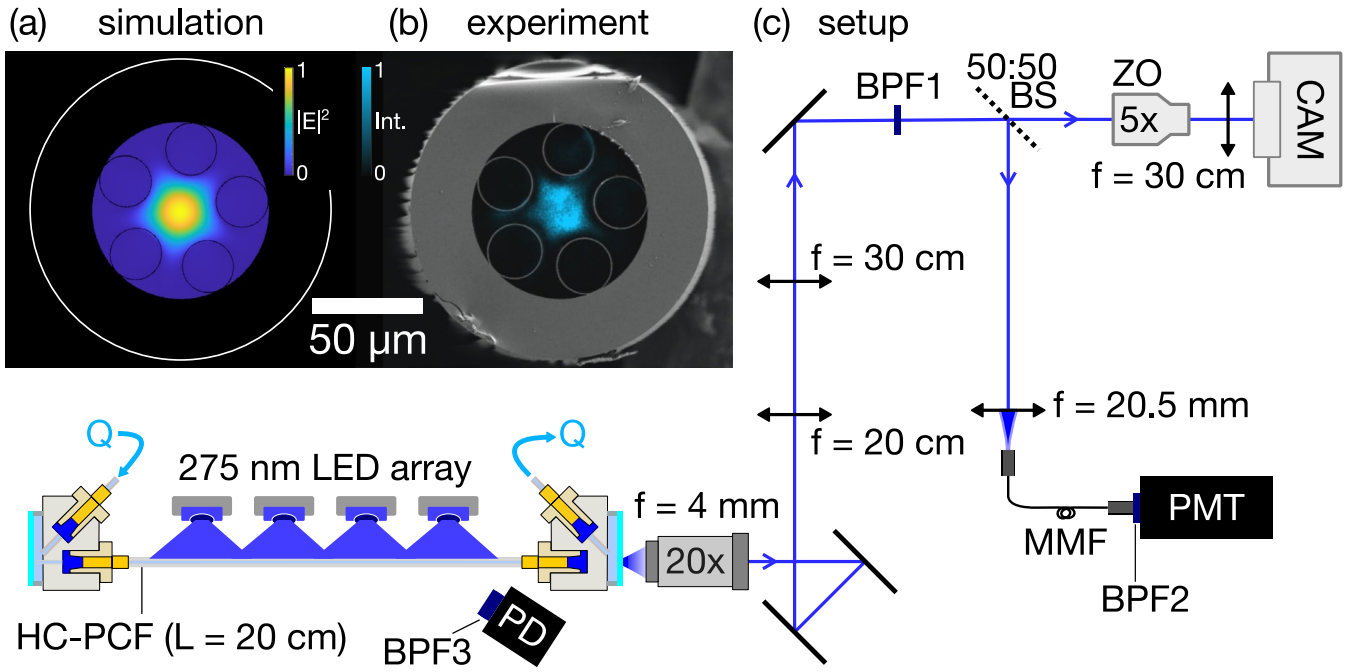

Figure 2 Intensity distribution through a water-filled antiresonant HC-PCF and experimental setup. (a) Calculated mode intensity distribution of the fundamental EH_{11} mode at $\lambda = 350$ nm superimposed onto the fibre geometry. (b) Measured mode intensity distribution, excited with a filtered halogen-deuterium lamp in a 20 cm long fibre, overlaid on a scanning electron micrograph (SEM) of the fibre. (c) Fluorescence detection setup. A protein solution continuously flows through the HC-PCF (Q). The protein's intrinsic fluorescence is excited by a transverse UV LED array, with excitation power monitored by a bandpass-filtered (BPF3) photodiode (PD). The collected fluorescence signal is imaged onto a CMOS camera (CAM1) using a 2*f* imaging system in combination with a zoom objective (ZO). A beam splitter (BS) sends half the light into a multimode fibre (MMF) coupled to a photomultiplier tube (PMT). Two identical bandpass filters BPF1 and BPF2 are used to select the BSA fluorescence band.

There are several advantages to the use of HC-PCF: first, their low transmission losses enable long-pathlength sensing in both gas and liquid samples[20,24], second, their transmission wavelength band can be tuned to UV wavelengths by changing the dimensions of the internal microstructure, third, HC-PCF can be manufactured from fused silica, which exhibits minimal fluorescence even at deep-UV wavelengths.[25]

Since their first realisation some twenty years ago[26], HC-PCF have been applied to low-volume high-sensitivity sensing in several fields.[20,27] For example, increased detection sensitivity from the extended path length of HC-PCFs has been demonstrated for UV absorption[28] and Raman spectroscopy of pharmacological compounds[29], leukemia cells[30], reaction mixtures [31], and battery electrolytes [32]. In fluorescence measurements, HCPCF can allow sensitivity in photochemical measurements down to attomole levels with less than 1 µL of sample [33]. The light confinement to the hollow core also allows two-photon excitation studied over long path lengths [34], the detection of weak singlet-oxygen fluorescence in the NIR range [29], or tracking of particles over extended timescales[35].

Early HC-PCFs employed relatively complex structures containing many narrow channels that significantly slow down the infiltration and exchange of liquid samples. Recent single-ring antiresonant HC-PCF designs [36], on the other hand, comprise fewer and larger side channels in the fibre structure and are therefore much easier to fabricate and infiltrate with liquid, and improve the microfluidic control of the infiltrated samples.

1.4 Protein sensing in HC-PCF

For protein sensing, HC-PCFs have been used by functionalising their surface.[37] Since the guidance properties of antiresonant HC-PCFs depend on wall thickness, protein adsorption causes a shift in their transmission spectrum. When the HC-PCF surface is functionalised, these multilayers become thick enough to be detectable from the resulting resonance shift.[38] Such transmission spectroscopy can be used to detect BSA protein in HC-PCF even without functionalisation at concentrations higher than 1g/L (15µM).[39]

HC-PCF surface can also be functionalised with antibodies that bind a given target protein, and a secondary fluorescently-labelled antibody is used for detection. Such surface-

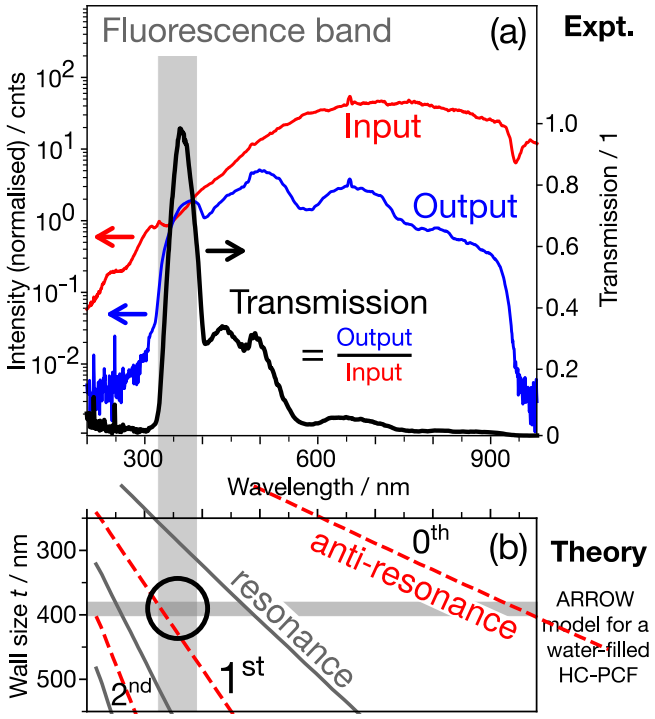

Figure 3 *(a)* Measured transmitted spectrum of a 25 cm long water-filled HC-PCF, using a halogen-deuterium light source. *(b)* The normalised transmission band is in excellent agreement with that predicted by the ARROW model for a 380 nm wall thickness, and centred near the intrinsic fluorescence emission wavelength of tryptophan (λ = 350 nm).

functionalisation approaches are promising due to their specificity, and are able to detect antioestrogen-α protein within a cell lysate at 1 g/L concentrations.[40]

However, while surface functionalisation can be used for biosensors targeting a specific protein, this method is not suitable for continuous measurements, as the adsorbed species needs to be removed between measurements to avoid saturation. More generally, all methods that rely on surface-binding, inherently detect proteins that are not in solution anymore. This limits their usefulness in the study of proteins in their native environment, where they can freely diffuse, make conformational changes and undergo protein-protein interactions, such as aggregation or binding to enzymes.

To overcome these limitations, we use optofluidic hollow-core photonic crystal fibres (HC-PCFs) to excite and monitor the intrinsic fluorescence of (label-free) and freely diffusing proteins under continuous flow. We utilise a custom-designed UV-guiding antiresonant HC-PCF to collect intrinsic fluorescence from a sub-µL sample of unmodified serum albumin protein, excited over 10 cm length of HC-PCF.

The fluorescence intensity is proportional to BSA concentration, demonstrating a new way to integrate label-free protein measurements with microfluidic systems and opening up possible applications in protein conformation and interaction studies.

Method

2.1 Experimental Setup

A setup was designed to use HC-PCFs for label-free protein analysis (Fig. 2c). A 25 cm long piece of HC-PCF is held between two metal cells that clamp and seal the fibre ends into liquid reservoirs with an internal dead volume of less than 20 µL. Connections to the cells allow the fibre to be infiltrated with liquid (Q) while retaining optical access through quartz windows. On one end of the fibre, a 50:50 beamsplitter (BS, Thorlabs BSW20R) is used to image the fibre facet onto a CMOS camera (CAM1, Photometrics Prime 95B) while also coupling half of the light into a multimode fibre (MMF, 50 µm, 0.22NA, Thorlabs FG050UGA), connected to a photomultiplier tube (PMT, Hamamatsu H1068201). A 2*f* imaging telescope is used to match the HC-PCF core diameter (30 µm) image to the MMF core diameter. Two 357 nm centre, 44 nm bandwidth bandpass filters (Semrock, FF01-357/44-25) are used to select the BSA fluorescence emission peak. An array of 275 nm LEDs (Bolb, S6060-DR250-W275-P100, see Suppl. Inf. for a measured spectrum and irradiance profile) is used to provide transverse excitation of the BSA solution in the HC-PCF core. Since the LED power output changes with LED temperature, the LED irradiance was monitored with a photodiode (Thorlabs, DET36A, with a bandpass filter 280 nm centre, 10 nm bandwidth), and all fluorescence spectra were referenced to the actual LED irradiance. The uniformity of excitation along the fibre is characterised in Suppl. Inf. S-4.

2.2 Hollow-core fibre design

The fibre used in this study is an antiresonant, single-ring HC-PCF. This type of HCPCF comprises several glass capillaries arranged along the inner wall of a larger circular capillary, forming a nearly-enclosed central channel (Fig. 2(b)). It was fabricated using the stack-and-draw process by combining thin-walled fused silica capillaries into the desired pattern and drawing it down to the desired fibre diameter and core wall thickness.[41] The literature describes the design criteria and performance of this type of fibre in detail.[42–44]

In the limit of core size much larger than wall thickness t, the antiresonant wavelengths $\lambda^{\mathrm{ar}}{}_{\mathrm{m}}$ at which transmission is maximal is given by:[45]

$$\lambda_m^{\mathrm{ar}} = \frac{4t}{2m+1}\sqrt{n_{\mathrm{silica}}^2 - n_{\mathrm{core}}^2}\,, \qquad m \in \mathbb{Z}_0^+$$

here m is the order of the resonance and n_{silica}, n_{core} are the wavelength-dependent refractive indices of the glass (Heraeus Suprasil 300) and the liquid medium in the core, respectively. Near the antiresonance wavelength, the core walls reflect light by constructive interference, resulting in guidance along the fibre.

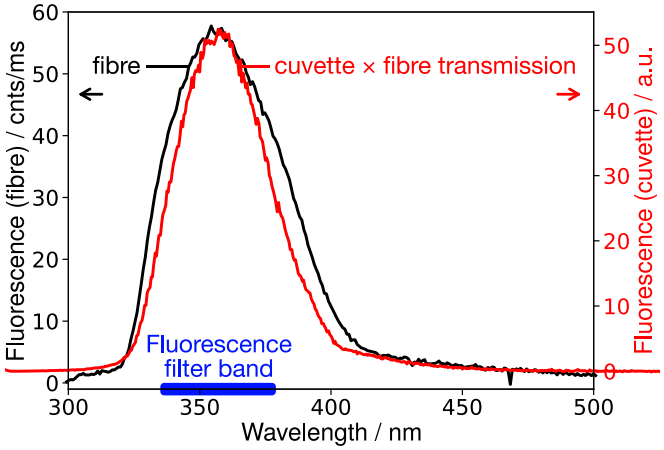

Figure 4 Comparison of fluorescence spectrum in the optofluidic HC-PCF to a commercial cuvette spectrophotometer. *(Black)* The fluorescence emerging from the HC-PCF when infiltrated with 10 µM BSA solution, referenced to the same fibre filled with buffer only. *(Red)* An identical solution is measured in a cuvette and adjusted for the fibre's guidance properties by multiplying by the measured transmission data from Fig. 3 (raw data in Suppl. Inf. Fig. S-5). The blue bar indicates the pass band filter used in the PMT measurements at lower concentrations (Fig. 5).

For the fibre used here, a circular central core region with a diameter D = 30 µm is surrounded by five capillaries with a diameter of d = 23 µm and average wall thickness t = 380 nm, corresponding to an antiresonance wavelength of λ^{ar}_1 = 350 nm, targeting the fluorescence emission wavelength (Fig. 3). The linear volumes are 7 nL cm^{-1} for the central core region and 49 nL cm^{-1} for the entire HC-PCF, resulting in volumes over the 10 cm excitation region of 70 nL and 490 nL, respectively (see Suppl. Inf. S.1).

The guidance properties of the fibres were confirmed experimentally by coupling a halogen-deuterium light source (Ocean Optics DH-2000) to a MMF (Thorlabs FG050UGA) whose core diameter of 50 µm closely matches that of the HC-PCF. The source MMF was then butt-coupled to a 25 cm length of HC-PCF filled with water by removing the left-hand liquid cell in Fig. 2. The HC-PCF liquid formed a water droplet acting as the interface between MMF and HC-PCF. The XYZ position of the MMF was adjusted to ensure that light was only launched into the HC-PCF core. A bandpass filter, centred at 350 nm, and a CMOS camera were used to confirm that UV light was guided in the water-filled hollow fibre core (Fig. 2). The transmitted spectrum of the fibre was obtained by coupling the collection MMF in Fig. 3 to a spectrometer (OceanOptics QE6500). The measured fibre output and source reference spectra were normalised to unity at 350 nm and divided by each other, with the resulting transmitted spectrum showing a peak value at 362 nm and a FWHM of 56 nm (Fig. 3).

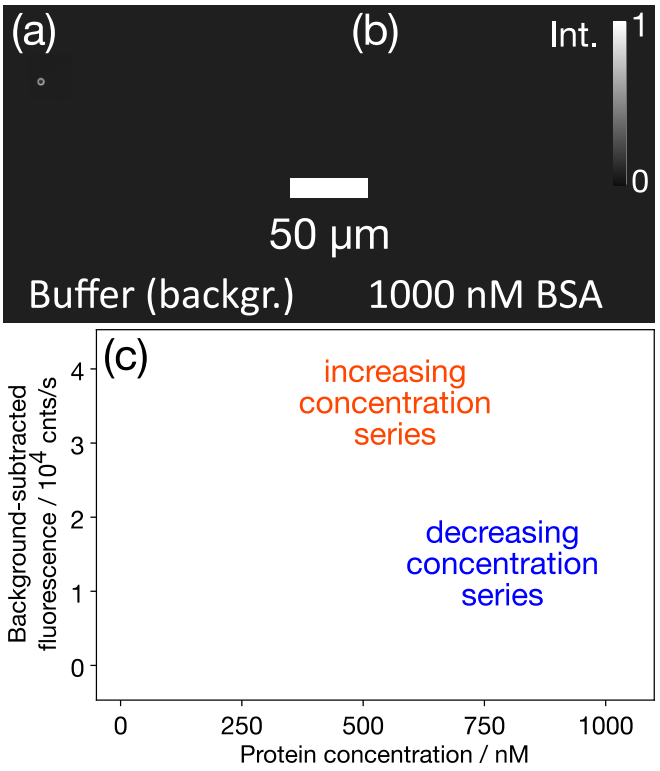

Figure 5 Intrinsic tryptophan fluorescence was measured under continuous flow in an optofluidic HC-PCF. *(a, b)* Camera images of bandpass-filtered fluorescence of (a) buffer only and (b) 1000 nM BSA relative to buffer. *(c)* Continuous flow fluorescence measurements were taken over 3 hours. The BSA concentration is increased from zero to 1000 nM (orange) and then back down to zero (blue). The linear fits show that the fluorescence signal is proportional to the concentration (increasing: R^2 = 0.994, decreasing: R^2 = 0.997, average: R^2 = 0.996).

The location of the transmission band is in excellent agreement with the transmission range predicted by the ARROW model and demonstrates that the fibre is optimised to the collection and guidance of tryptophan's intrinsic fluorescence emission band (λ = 350 nm). In addition to the ability to successfully engineer transmission properties in the ultraviolet, the relatively large channels in the structure facilitate continuous flow experiments such as the one demonstrated here.

2.3 Protein sample preparation and infiltration

Protein solutions with different concentrations were prepared from lyophilised bovine serum albumin powder (BSA, Sigma-Aldrich) dissolved into phosphate-buffered saline (PBS, Lonza). BSA is a globular protein (r_H = 3.5 nm, m = 66.5 kDa) containing two tryptophan units.[46] Samples were vortexed for three seconds before being filled into glass syringes and injected into the setup using a syringe pump (NE-1000, New Era Pump Systems) at a flow rate of 5 µL min^{-1}. To minimise surface adhesion, all wetted surfaces in the

fluidic system are made of either glass, PEEK polymer, or stainless steel. The internal volume of the HC-PCF is 49 nL cm^{-1} per unit length leading to an average flow velocity of ca. 1.7 cm s^{-1} through the fibre. For the concentration series in Fig. 5, the flow was stopped at specific times to exchange syringes. The stabilisation time of the fluidic system after each syringe exchange was approximately 10 min, after which the fluorescence signal stayed approximately constant, and data were collected.

Results

Our key results are 1) the spectroscopic analysis of a BSA solution in HC-PCF under continuous flow, finding the spectrum to be similar to cuvette spectra when accounting for the previously-measured guidance properties of the fibre; and 2) the quantification of lower concentrations of BSA, characterising the linearity and repeatability (hysteresis) of our measurement for over three hours.

3.1 Spectroscopy in HC-PCF and comparison to cuvette

To test whether the HC-PCF affects the BSA fluorescence spectrum compared to large-volume bulk experiments, a 10 µM concentration of BSA (ten times higher than in the experiments below) was infiltrated into the fibre. The light emerging from the fibre was analysed by a spectrometer (OceanOptics QE6500) using an integration time of 5 s, i.e. the setup from Fig. 2 was used but with the spectrometer taking the place of the PMT, and bandpass filters removed. The irradiance of the transverse LED was set to 5 mW cm^{-2}.

Fig. 4 shows the BSA fluorescence spectrum, which is recorded after subtracting a buffer-only background spectrum, compared to a cuvette measurement in a commercial system (Cary Eclipse Fluorescence Spectrophotometer). To directly compare the broadband free-space cuvette measurements to the waveguiding HC-PCF's wavelength-selective guidance (optimised for 350 nm fluorescence collection), we multiply the cuvette data by the normalised fibre transmission from Fig. 3. We also show the raw data in the Suppl. Inf. Fig. S-6.

3.2 Concentration series

Next, the ability of this setup to measure BSA fluorescence at much lower concentrations was explored (Fig. 5). Two bandpass filters select 64 % (Fig. 4) of the tryptophan fluorescence band between 335 nm to 379 nm. Then, by changing between syringes with different BSA aliquots, the concentration is increased from zero to 1000 nM and back down to zero. The PMT count rate, subtracting the zero concentration value, increased linearly with BSA concentration (Fig. 5). The PMT trace from which these data points were taken after each sample change, allowing the system to establish equilibrium before each datum, is shown in the Suppl. Inf. Fig. S-7.

Results

The comparison between HC-PCF and cuvette data in Fig. 4 showed that, despite the 1000 times smaller sample volume in the fibre (microliters vs. millilitres), the peak position and shape of the fluorescence spectra in the PCF and cuvette agree to within 5 nm, when taking into account the fibre's transmission spectrum. The spectral shape agrees with that of tryptophan found in the literature [47], indicating that tryptophan is the dominant source of intrinsic protein fluorescence in our experiments. Tyrosine, an amino acid with a slightly higher quantum yield than tryptophan and an absorption peak at 275 nm, hence more readily excited by our light source, is also present in BSA. However, the efficient Förster resonant energy transfer (FRET) from tyrosine to tryptophan diminishes the resulting fluorescence contribution, found to be less than 10 % in a study on interferon-γ protein[48], making tryptophan the dominant fluorophore.

Notably, fluorescence is not only guided in the core region but also in the five side capillaries (Fig. 5 (a, b)). This is consistent with the ARROW model, which can also be applied to each side capillary. Notably, these capillaries show LP_{11}-like modes whose orientation is in good agreement with finite difference frequency domain simulations of the fibre structure (Fig. S-2).

The intrinsic fluorescence intensity increases linearly with protein concentration (Fig. 5), indicating that internal re-absorption due to long path length does not play a significant role at the low BSA concentrations studied. Furthermore, data points taken during the decreasing concentration series show a similar or slightly smaller fluorescence signal than their increasing concentration series counterparts. This absence of hysteresis indicates that unwanted adsorption of BSA proteins onto the fibre walls does not occur. The cause of the small but continuous reduction in baseline fluorescence signal over time (ca. 4 % h^{-1}, Fig. S-7), can be attributed to slow thermal drift in the optomechanical components due to the residual waste heat of the LEDs that was not sufficiently extracted from the setup.

Conclusion

Optofluidic HC-PCFs can detect and quantify BSA concentrations in the 100 – 1000 nM range by label-free fluorescence emitted at 350 nm. Measurements can be taken under continuous flow from detection volumes of less than 1 µL, making the method compatible with low-volume microfluidic techniques. The obtained fluorescence spectra agree with reference data taken from a 3000 times larger sample volume in a cuvette, and fluorescence increased linearly with concentration and minimal hysteresis was observed over three hours of continuous measurements.

The reliability of the setup for long-term, low-concentration measurements could be further improved by

reducing the temperature-related drift in baseline fluorescence signal with water- or air-cooling of the LED and camera-electronics.

This method will be of interest to studies with aggregating protein solutions. Due to the very small detection volume, a continuous flow of samples could be extracted from an aggregating solution, enabling uninterrupted continuous data collection. Proteins are known to change their fluorescence properties through conformational changes. For example, conformations that expose the tryptophan groups to a solvent can result in quenching [13–15]. As the approach allows proteins to be monitored continuously in their native buffer conditions and without labels, it is expected to provide new insights into aggregation kinetics.To enable high-throughput screening measurements, integrating the hollow-core fibres with existing microfluidic chips is key. Previous work has shown the feasibility of connecting HC-PCF-based microreactors to a mass spectrometer using low-dead volume coupling cells [49]. Similar techniques can integrate the label-free fibre sensor with a wide range of on-chip protein biophysics [50].

The UV fluorescence excitation could be further improved in several ways. First, modulating the output power of the LEDs could enable lock-in detection schemes that would further improve the signal-to-noise ratio. Second, the irradiation intensity, and thus the fluorescence signal, could be increased by increasing the number of LEDs positioned along the HC-PCF and by adding reflective optics underneath the fibre.

The detection efficiency of the intrinsic fluorescence, on the other hand, could be improved by increasing the collection NA of the fibre. This can be achieved by a double-clad HC-PCF design or by coating the fibre's outer surface with a low-index polymer coating, creating a multimode optical fibre that will collect a larger fraction of the intrinsic fluorescence, enabling label-free detection at even lower protein concentrations.

Conflict of interest statement

The authors have declared that no conflicting interests exist.

Acknowledgements

The authors wish to thank the Engineering and Physical Sciences Research Council (EP/L015889/1) and the Leverhulme Trust (Research Project Grant RPG-2018-256) for financial support during the period of this research. For the purpose of open access, the author has applied a Creative Commons Attribution (CC BY 4.0) licence to any Author Accepted Manuscript version arising from this submission.

Data availability statement

The data that support the findings of this study are available upon reasonable request from the authors.

References

[1] Knowles T P J, Vendruscolo M and Dobson C M 2015 The physical basis of protein misfolding disorders *Physics Today* **68** 36–41

[2] Michaels T C T, Šarić A, Meisl G, Heller G T, Curk S, Arosio P, Linse S, Dobson C M, Vendruscolo M and Knowles T P J 2020 Thermodynamic and kinetic design principles for amyloid-aggregation inhibitors *Proc Natl Acad Sci USA* **117** 24251–7

[3] Yates E V, Müller T, Rajah L, De Genst E J, Arosio P, Linse S, Vendruscolo M, Dobson C M and Knowles T P J 2015 Latent analysis of unmodified biomolecules and their complexes in solution with attomole detection sensitivity *Nature Chem* **7** 802–9

[4] Li D 2015 *Encyclopedia of Microfluidics and Nanofluidics* (New York, NY: Springer New York)

[5] Valeur B 2009 Molecular Fluorescence *digital Encyclopedia of Applied Physics* ed Wiley-VCH Verlag GmbH & Co. KGaA (Weinheim, Germany: Wiley-VCH Verlag GmbH & Co. KGaA) pp 477–531

[6] Walter N G 2010 *Fluorescence based approaches* (Amsterdam: Elsevier, Acad. Press)

[7] Toseland C P 2013 Fluorescent labeling and modification of proteins *J Chem Biol* **6** 85–95

[8] Weiss S 1999 Fluorescence Spectroscopy of Single Biomolecules *Science* **283** 1676–83

[9] Zhang J, Campbell R E, Ting A Y and Tsien R Y 2002 Creating new fluorescent probes for cell biology *Nat Rev Mol Cell Biol* **3** 906–18

[10] Saar K-L, Yates E V, Müller T, Saunier S, Dobson C M and Knowles T P J 2016 Automated Ex Situ Assays of Amyloid Formation on a Microfluidic Platform *Biophysical Journal* **110** 555–60

[11] Szmacinski H, Ray K and Lakowicz J R 2009 Metal-enhanced fluorescence of tryptophan residues in proteins: Application toward label-free bioassays *Analytical Biochemistry* **385** 358–64

[12] Lakowicz J R 1991 *Topics in fluorescence spectroscopy* (New York: Plenum Press)

[13] Moriyama Y, Ohta D, Hachiya K, Mitsui Y and Takeda K 1996 Fluorescence behavior of tryptophan residues of bovine and human serum albumins in ionic surfactant solutions: A comparative study of the two and one tryptophan(s) of bovine and human albumins *J Protein Chem* **15** 265–72

[14] Vivian J T and Callis P R 2001 Mechanisms of Tryptophan Fluorescence Shifts in Proteins *Biophysical Journal* **80** 2093–109

[15] Ghisaidoobe A and Chung S 2014 Intrinsic Tryptophan Fluorescence in the Detection and Analysis of Proteins: A Focus on Förster Resonance Energy Transfer Techniques *IJMS* **15** 22518–38

[16] Weber G 1952 Polarization of the fluorescence of macromolecules. 1. Theory and experimental method *Biochemical Journal* **51** 145–55

[17] Toprakcioglu Z, Challa P, Xu C and Knowles T P J 2019 Label-Free Analysis of Protein Aggregation and Phase Behavior *ACS Nano* **13** 13940–8

[18] Challa P K, Peter Q, Wright M A, Zhang Y, Saar K L, Carozza J A, Benesch J L P and Knowles T P J 2018 Real-Time Intrinsic Fluorescence Visualization and Sizing of Proteins and Protein Complexes in Microfluidic Devices *Anal. Chem.* **90** 3849–55

[19] Hawkins A R and Schmidt H 2008 Optofluidic waveguides: II. Fabrication and structures *Microfluid Nanofluid* **4** 17–32

[20] Cubillas A M, Unterkofler S, Euser T G, Etzold B J M, Jones A C, Sadler P J, Wasserscheid P and Russell P St J 2013 Photonic crystal fibres for chemical sensing and photochemistry *Chem. Soc. Rev.* **42** 8629

[21] Zhang Y, Kenarangi F, Zhang H, Vaziri S, Li D, Pu X and Sun Y 2020 Versatile Optofluidic Solid-Core/Liquid-Cladding Waveguide Based on Evanescent Wave Excitation *Anal. Chem.* **92** 14983-89

[22] Li Z, Liao C, Chen D, Song J, Jin W, Peng G-D, Zhu F, Wang Y, He J and Wang Y 2017 Label-free detection of bovine serum albumin based on an in-fiber Mach-Zehnder interferometric biosensor *Opt. Express* **25** 17105

[23] Russell P St J 2006 Photonic-Crystal Fibers *J. Lightwave Technol.* **24** 4729–49

[24] Smolka S, Barth M and Benson O 2007 Highly efficient fluorescence sensing with hollow core photonic crystal fibers *Opt. Express* **15** 12783

[25] Schulze P, Ludwig M, Kohler F and Belder D 2005 Deep UV Laser-Induced Fluorescence Detection of Unlabeled Drugs and Proteins in Microchip Electrophoresis *Anal. Chem.* **77** 1325–9

[26] Knight J C, Birks T A, Russell P St J and Atkin D M 1996 All-silica single-mode optical fiber with photonic crystal cladding *Opt. Lett.* **21** 1547

[27] Calcerrada M, García-Ruiz C and González-Herráez M 2015 Chemical and biochemical sensing applications of microstructured optical fiber-based systems: Chemical and biochemical sensing applications . . . *Laser & Photonics Reviews* **9** 604–27

[28] Nissen M, Doherty B, Hamperl J, Kobelke J, Weber K, Henkel T and Schmidt M 2018 UV Absorption Spectroscopy in Water-Filled Antiresonant Hollow Core Fibers for Pharmaceutical Detection *Sensors* **18** 478

[29] Wolf S, Frosch T, Popp J, Pletz M W and Frosch T 2019 Highly Sensitive Detection of the Antibiotic Ciprofloxacin by Means of Fiber Enhanced Raman Spectroscopy *Molecules* **24** 4512

[30] Khetani A, Momenpour A, Alarcon E I and Anis H 2015 Hollow core photonic crystal fiber for monitoring leukemia cells using surface enhanced Raman scattering (SERS) *Biomed. Opt. Express* **6** 4599

[31] Schorn F, Aubermann M, Zeltner R, Haumann M and Joly N Y 2021 Online Monitoring of Microscale Liquid-Phase Catalysis Using in-Fiber Raman Spectroscopy *ACS Catal.* **11** 6709–14

[32] Miele E, Dose W M, Manyakin I, Frosz M H, Ruff Z, De Volder M F L, Grey C P, Baumberg J J and Euser T G 2022 Hollow-core optical fibre sensors for operando Raman spectroscopy investigation of Li-ion battery liquid electrolytes *Nat Commun* **13** 1651

[33] Williams G O S, Euser T G, Russell P S J and Jones A C 2013 Spectrofluorimetry with attomole sensitivity in photonic crystal fibres *Methods Appl. Fluoresc.* **1** 015003

[34] Williams G O S, Euser T G, Arlt J, Russell P St J and Jones A C 2014 Taking Two-Photon Excitation to Exceptional Path-Lengths in Photonic Crystal Fiber *ACS Photonics* **1** 790–3

[35] Förster R, Weidlich S, Nissen M, Wieduwilt T, Kobelke J, Goldfain A M, Chiang T K, Garmann R F, Manoharan V N, Lahini Y and Schmidt M A 2020 Tracking and Analyzing the Brownian Motion of Nano-objects Inside Hollow Core Fibers *ACS Sens.* **5** 879–86

[36] Hartung A, Kobelke J, Schwuchow A, Wondraczek K, Bierlich J, Popp J, Frosch T and Schmidt M A 2014 Double antiresonant hollow core fiber – guidance in the deep ultraviolet by modified tunneling leaky modes *Opt. Express* **22** 19131

[37] Ermatov T, Skibina J S, Tuchin V V and Gorin D A 2020 Functionalized Microstructured Optical Fibers: Materials, Methods, Applications *Materials* **13** 921

[38] Giovanardi F, Cucinotta A, Rozzi A, Corradini R, Benabid F, Rosa L and Vincetti L 2019 Hollow Core Inhibited Coupling Fibers for Biological Optical Sensing *J. Lightwave Technol.* **37** 2598–604

[39] Ermatov T, Noskov R E, Machnev A A, Gnusov I, Atkin V, Lazareva E N, German S V, Kosolobov S S, Zatsepin T S, Sergeeva O V, Skibina J S, Ginzburg P, Tuchin V V, Lagoudakis P G and Gorin D A 2020 Multispectral sensing of biological liquids with hollow-core microstructured optical fibres *Light Sci Appl* **9** 173

[40] Padmanabhan S, Shinoj V K, Murukeshan V M and Padmanabhan P 2010 Highly sensitive optical detection of specific protein in breast cancer cells using microstructured fiber in extremely low sample volume *J. Biomed. Opt.* **15** 017005

[41] Uebel P, Günendi M C, Frosz M H, Ahmed G, Edavalath N N, Ménard J-M and Russell P St J 2016 Broadband robustly single-mode hollow-core PCF by resonant filtering of higher-order modes *Opt. Lett.* **41** 1961

[42] Archambault J-L, Black R J, Lacroix S and Bures J 1993 Loss calculations for antiresonant waveguides *J. Lightwave Technol.* **11** 416–23

[43] Selim Habib Md, Markos C and Amezcua-Correa R 2021 Impact of cladding elements on the loss performance of hollow-core anti-resonant fibers *Opt. Express* **29** 3359

[44] Sakr H, Bottrill K R H, Taengnoi N, Wheeler N V, Petropoulos P, Richardson D J, Poletti F, Hong Y, Bradley T D, Jasion G T, Hayes J R, Kim H, Davidson I A, Fokoua E N and Chen Y 2020 Interband Short Reach Data Transmission in Ultrawide Bandwidth Hollow Core Fiber *J. Lightwave Technol.* **38** 159–65

[45] Litchinitser N M, Abeeluck A K, Headley C and Eggleton B J 2002 Antiresonant reflecting photonic crystal optical waveguides *Opt. Lett.* **27** 1592

[46] Rosenoer V M, Oratz M and Rothschild M A 1977 *Albumin structure, function and uses* (Oxford ; New York: Pergamon Press)

[47] Lakowicz J R 2006 Protein Fluorescence *Principles of Fluorescence Spectroscopy* (Boston, MA: Springer US) pp 529–75

[48] Boteva R, Zlateva T, Dorovska-Taran V, Visser A J W G, Tsanev R and Salvato B 1996 Dissociation Equilibrium of Human Recombinant Interferon γ *Biochemistry* **35** 14825–30

[49] Unterkofler S, McQuitty R J, Euser T G, Farrer N J, Sadler P J and Russell P St J 2012 Microfluidic integration of photonic crystal fibers for online photochemical reaction analysis *Opt. Lett.* **37** 1952

[50] Charmet J, Arosio P and Knowles T P J 2018 Microfluidics for Protein Biophysics *Journal of Molecular Biology* **430** 565–80

Supplementary Information for: Label-free monitoring of proteins in optofluidic hollow-core photonic crystal fibres

Received xxxxxx
Accepted for publication xxxxxx
Published xxxxxx

S.1 Geometrical model for fibre hydrodynamics and flow

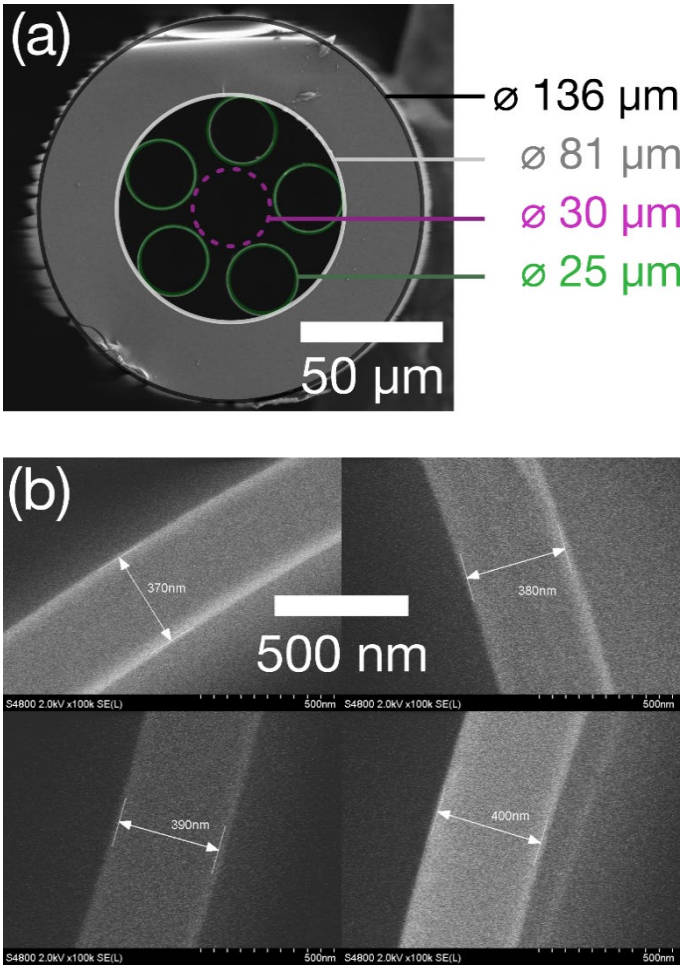

Figure S-1. (a) SEM with overlaid geometry showing the diameters for the whole fibre (black), the hollow channel (white), the central core region (purple) and the five identical cladding capillaries (green). (b) SEMs of the cladding capillaries showing their strut thicknesses.

The fibre used in these experiments is a single-ring hollow-core photonic crystal fibre with a geometry as measured from the SEM image shown in Fig. S-1. The central core region is defined as the circle circumscribed by the five cladding capillaries as drawn. We model the hydrodynamics of the fibre as parallel cylindrical flow channels, neglecting the in-between regions with much higher surface-to-volume ratios. Therefore, due to viscous drag from the walls, we contribute much less to the overall flow. Using the equation for the hydrodynamic resistance $R_{\text{hyd},\bigcirc}$ of a cylindrical flow channel of length L and radius r with a fluid of dynamic viscosity μ (water: 1.0 mPa s [1](Tbl. B.2)),

$$R_{\text{hyd},\bigcirc} = \frac{8}{\pi}\mu L r^{-4}, \quad \text{(A.1)}$$

the hydrodynamic resistance per unit length for the diameters given are

$$R_{\text{hyd,core}}/L = 8.4\,\text{kPa}/(\text{cm}\cdot\mu\text{L}/\text{min}) \quad \text{(A.2)}$$

and

$$R_{\text{hyd,capillary}}/L = 17.4\,\text{kPa}/(\text{cm}\cdot\mu\text{L}/\text{min}). \quad \text{(A.3)}$$

Next, modelling the flow through the entire fibre as the hydrodynamic circuit of the core and five capillaries all in parallel results in a linear hydrodynamic resistance of

$$R_{\mathrm{hyd,fibre}}/L = \left(1/R_{\mathrm{hyd,core}} + 5 \cdot 1/R_{\mathrm{hyd,capillary}}\right)^{-1}/L \quad \text{(A.4)}$$

$$= 2.5\,\mathrm{kPa}/(\mathrm{cm} \cdot \mu\mathrm{L}/\mathrm{min}). \quad \text{(A.5)}$$

The ratio of the hydrodynamic resistance of the core channel to all capillaries together is 8.4 : (5/17.4)−1 ≈ 2.4 : 1. Hence, since the same pressure is applied to all flow channels, the flow rate in the core is 2.4 times lower than the sum of the capillaries; i.e. the core region carries $(1/R_{hyd,core})/(1/R_{hyd,fibre}) \approx 30$ % of the fibre's total flow rate.

S.2. Waveguide mode simulations

A full-wave finite difference frequency domain (FDFD) solver has been used to determine the propagation-invariant modes guided in this waveguide geometry. The waveguide is assumed to be translationally invariant, allowing Maxwell's equations to be discretised using a two-dimensional Yee cell. This yields an eigenvalue equation which is solved using Arnoldi iteration to obtain the mode profiles and propagation constants. These calculations are described in greater depth in [2].

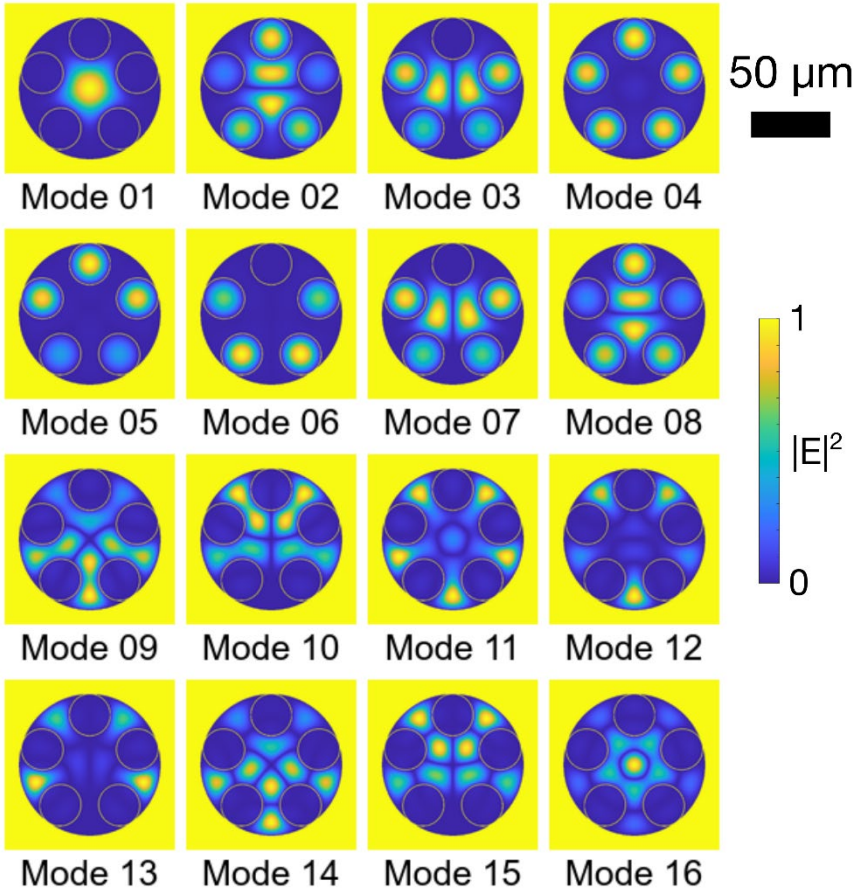

Figure S-2a. A subset of propagation-invariant modes guided in the fibre. The modes have been calculated using a custom FDFD model [2].

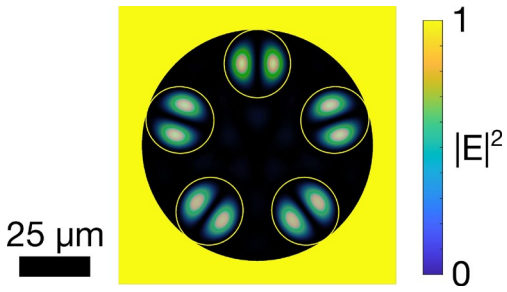

Figure S-2b. Superposition of three higher-order HC-PCF modes showing guidance in the capillaries. These capillaries, which form the cladding that gives the core region its guidance (see Fig. 2), also support their own modes. While, for the individual capillaries, they are LP11 modes, from the perspective of the entire HC-PCF, these are superpositions of several higher-order modes. In yellow is the geometric model used for simulations.

S.3. Excitation spectrum

A spectrum of the LEDs used for exciting intrinsic protein fluorescence.

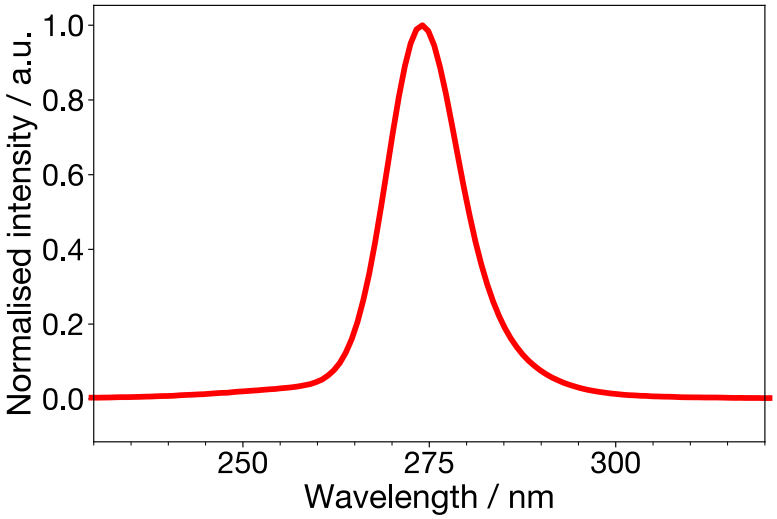

Figure S-3. Excitation source spectrum. A multimode fibre (MMF, 50 µm, 0.22NA) is placed in the HC-PCF plane 5 cm away from the fibre, facing the excitation source. Its output is analysed by an OceanOptics QE6500 spectrometer (integration time 500 ms). The MMF position was chosen not to saturate the spectrometer. Since the LEDs have a weak temperature–wavelength dependence, they were operated at a constant power level. For the same reason, the LEDs' temperature was allowed to stabilise first.

S.4. Line scan of the excitation source

Irradiance measurements of the excitation source (four LEDs) were taken at the fibre plane along the fibre axis.

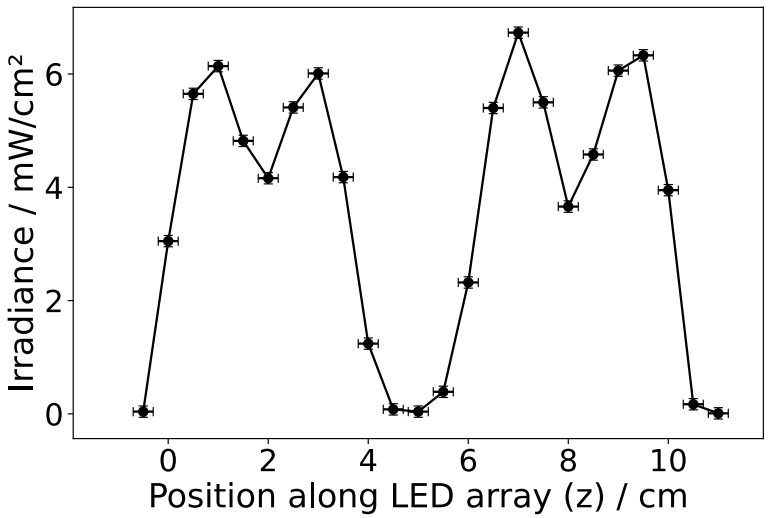

Figure S-4. Line scan of excitation irradiance along the fibre. The 4 LEDs were arranged in a 2-and-2 pattern of 2 cm position spacing, with the in-between position left empty. Irradiance was measured using a calibrated photodiode power meter (detector area 1 cm^2) with a 280 nm centre, 20 nm width bandpass filter. LEDs were turned on only briefly for each measurement datum and allowed to cool in between, such that they did not heat up and decrease their power output significantly; hence this graph is for peak power output

S.5. Measurement of BSA in a spectrophotometer

Comparison of 275 nm excitation (as with the LEDs used in this work, see Fig. S-3) compared to 280 nm (BSA absorption peak), showing a slight, ca. 10 % decrease in fluorescence emission (peak value).

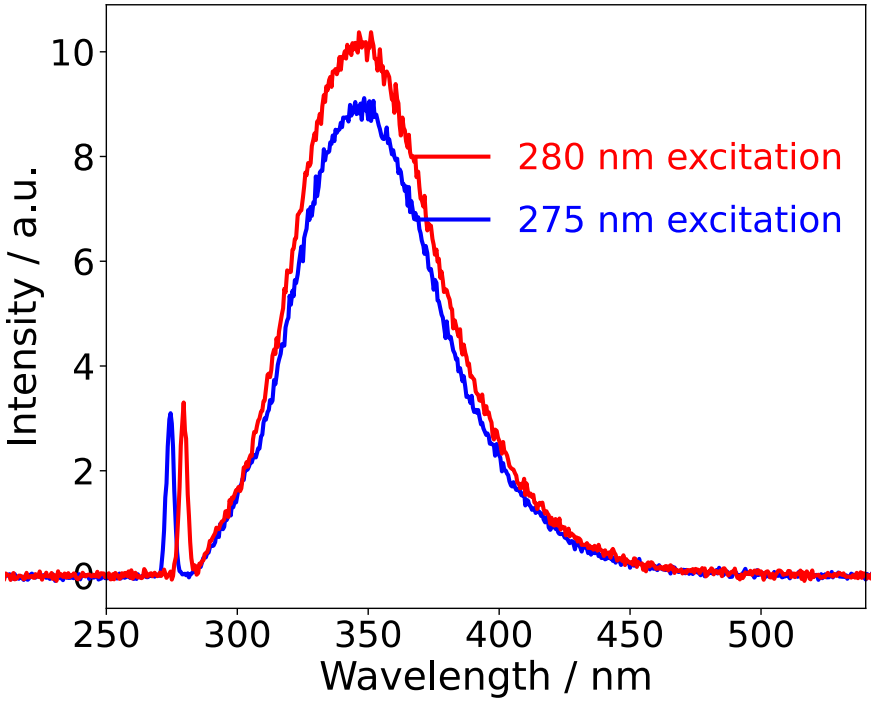

Figure S-5. Intrinsic protein fluorescence of BSA quantified in a commercial cuvette spectrophotometer (Cary Eclipse Fluorescence Spectrophotometer). 3 mL of a 1 µM solution of BSA is measured in a quartz cuvette in a perpendicular excitation-emission configuration, quantifying the difference between 275 nm excitation (as in our experiments) compared to 280 nm (absorption peak). Slit widths 2.5 nm, scan speed 60 nm min^{-1}. The concentration was chosen to give a calculated 10 % transmission at 280 nm.

S.6. Full data for the fluorescence spectra

Fluorescence spectra of 10 μM BSA in PBS in HC-PCF (black) and cuvette (red). Multiplying the cuvette data with the HC-PCF's transmission spectrum (Fig. 3) yields Fig. 4 in the main text.

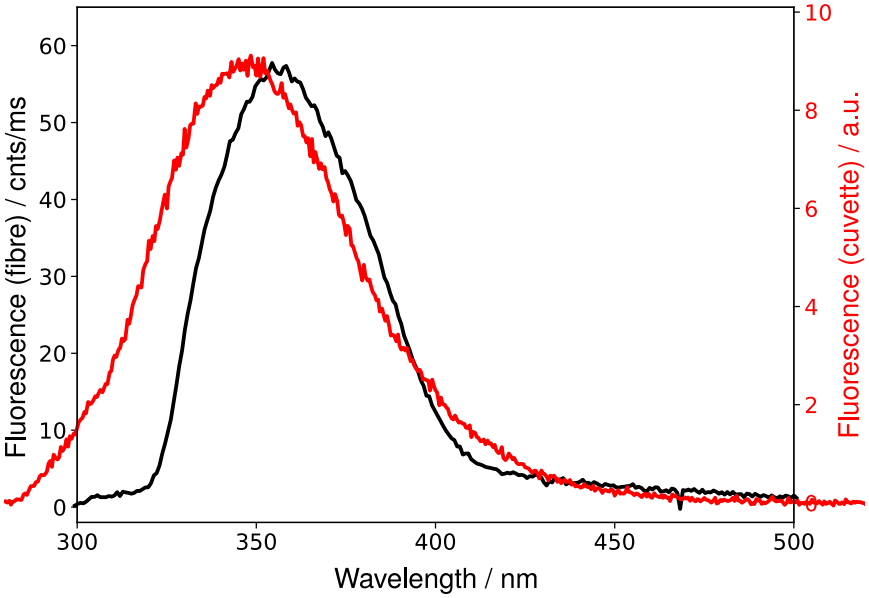

Figure S-6. Data in Fig. 4 before accounting for the fibre guidance properties.

S.7. Full data for the concentration series

The full data acquired for the main experiment, resulting in Fig. 5, with red dots indicating the data points used in the fluorescence linearity plot.

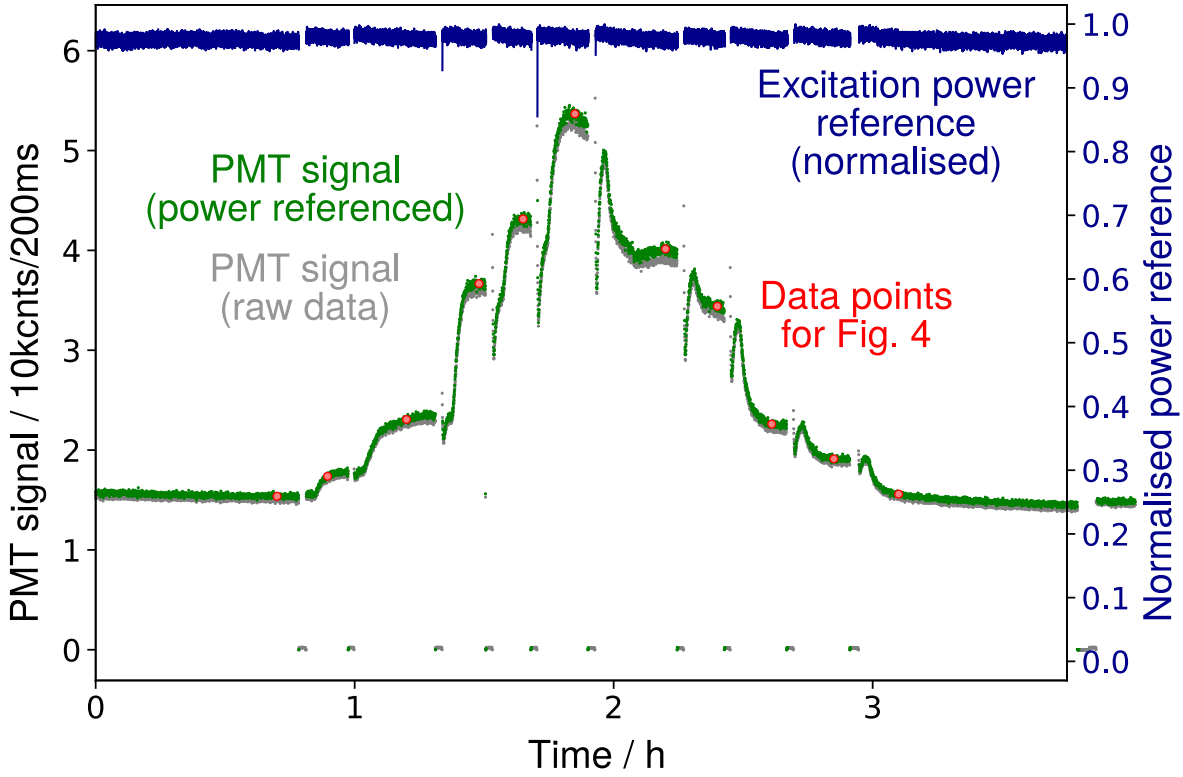

Figure S-7. Time trace of intrinsic fluorescence intensity during sample exchanges. The excitation is turned off during each sample exchange, and the PMT signal drops to its background count rate. The excitation power is slightly higher whenever turned on again, as the efficiency of the LEDs decreases with temperature. A large heatsink ensures stable operation after a short warmup period. Nonetheless, the fluorescence signal as measured by the PMT is corrected by dividing by the normalised excitation power. For visual clarity, only every tenth data point is plotted of the 72251 PMT data points acquired over 3 hours.

References

[1] Munson B R, Okiishi T H, Huebsch W W and Rothmayer A P 2013 *Fundamentals of fluid mechanics* (Hoboken, NJ: John Wiley & Sons, Inc)

[2] Mouthaan R, Christopher P J, Pinnell J, Frosz M, Gordon G, Wilkinson T D and Euser T G 2022 Efficient Excitation of High-Purity Modes in Arbitrary Waveguide Geometries *J. Light. Technol.* **40** 1150–60